Dry-wet digital etching of Ge1−xSnx

Colleen K. Shang, Vivian Wang, Robert Chen, Suyog Gupta, Yi-Chiau Huang, James J. Pao, Yijie Huo, Errol Sanchez, Yihwan Kim, Theodore I. Kamins, and James S. Harris

Citation: Applied Physics Letters **108**, 063110 (2016); doi: 10.1063/1.4941800
View online: http://dx.doi.org/10.1063/1.4941800
View Table of Contents: http://scitation.aip.org/content/aip/journal/apl/108/6?ver=pdfcov
Published by the AIP Publishing

Articles you may be interested in

Synthesis of Ge1−xSnx alloys by ion implantation and pulsed laser melting: Towards a group IV direct bandgap material
J. Appl. Phys. **119**, 183102 (2016); 10.1063/1.4948960

Systematic study of Ge1−xSnx absorption coefficient and refractive index for the device applications of Si-based optoelectronics
J. Appl. Phys. **119**, 103106 (2016); 10.1063/1.4943652

Effects of uniaxial strain on electron effective mass and tunneling capability of direct gap Ge1−xSnx alloys
AIP Advances **6**, 015102 (2016); 10.1063/1.4939816

Raman study of strained Ge1−xSnx alloys
Appl. Phys. Lett. **98**, 261917 (2011); 10.1063/1.3606384

Measurement of the direct energy gap of coherently strained Sn x Ge 1−x / Ge(001) heterostructures
Appl. Phys. Lett. **77**, 3418 (2000); 10.1063/1.1328097

AIP Applied Physics Reviews
NEW Special Topic Sections
NOW ONLINE
Lithium Niobate Properties and Applications: Reviews of Emerging Trends
AIP Applied Physics Reviews

Reuse of AIP Publishing content is subject to the terms at: https://publishing.aip.org/authors/rights-and-permissions. Download to IP: 128.103.220.217 On: Thu, 26 May 2016 21:13:39

APPLIED PHYSICS LETTERS 108, 063110 (2016)

Dry-wet digital etching of $Ge_{1-x}Sn_x$

Colleen K. Shang,[1,a)] Vivian Wang,[2] Robert Chen,[2] Suyog Gupta,[2] Yi-Chiau Huang,[3] James J. Pao,[4] Yijie Huo,[2] Errol Sanchez,[3] Yihwan Kim,[3] Theodore I. Kamins,[2] and James S. Harris[2]

[1]*Department of Materials Science and Engineering, Stanford University, Stanford, California 94305, USA*
[2]*Department of Electrical Engineering, Stanford University, Stanford, California 94305, USA*
[3]*Applied Materials, Inc., 974 E. Arques Avenue, Sunnyvale, California 94085, USA*
[4]*OEpic Semiconductors Inc., 1231 Bordeaux Drive, Sunnyvale, California 94089, USA*

(Received 6 March 2015; accepted 30 January 2016; published online 11 February 2016)

The development of a precise micromachining process for $Ge_{1-x}Sn_x$ has the potential to enable both the fabrication and optimization of $Ge_{1-x}Sn_x$-based devices in photonics and microelectromechanical systems. We demonstrate a digital etching scheme for $Ge_{0.922}Sn_{0.078}$ based on a two-stage, highly selective CF_4 plasma dry etch and HCl wet etch. Using X-Ray Reflectivity, we show consistent etch control as low as 1.5 nm per cycle, which is defined as one dry etch step followed by one wet etch step. The etch rate increases to 3.2 nm per cycle for a longer dry etch time due to physical sputtering contributions, accompanied by an increase in RMS surface roughness. By operating within a regime with minimal sputtering, we demonstrate that good digital etch depth control and surface quality can be achieved using this technique. *© 2016 AIP Publishing LLC*. [http://dx.doi.org/10.1063/1.4941800]

Recent predictions and demonstrations that 6%–9% Sn is sufficient to transform germanium-tin ($Ge_{1-x}Sn_x$) into a direct band gap material has led to a growing interest in this system for the development of silicon-compatible photonic and optoelectronic devices.[1–3] With the continued trend of device scaling for improved performance and large-scale integration, control over critical feature sizes is becoming arguably more important. Developing a highly selective micromachining technique to precisely define small features as well as exercise post-processing control enables the tuning and optimization of Ge and $Ge_{1-x}Sn_x$-based devices for achieving targeted device performance on these length scales. Moreover, such a technique provides an avenue for the design and application of suspended $Ge_{1-x}Sn_x$ structures that can be leveraged in microelectromechanical systems (MEMS).

As a complement to growth techniques with atomic layer control, digital etching is a method of achieving precise control of material removal through cycles of self-limiting or highly selective processes. The utility of digital etching can range from tuning photonic crystal resonances[4,5] to achieving reproducible gate recess etching in transport devices such as HEMTs and MOSFETs.[6–8] In conventional timed etches, the etch depth is often difficult to control in the absence of a stopping mechanism and can be subject to variation over process runs. In contrast, digital etching has the advantage of predictable etch rates governed by cycle iterations instead of time.

Various digital etching schemes have already been developed in various materials systems using combinations of dry and wet etching processes. In III-V systems achieving etch rates of 1–3 nm per cycle, typical procedures involve an initial oxidation step, either by a chemical oxidizing agent or by native oxide formation in plasma and atmospheric conditions, followed by an acid wet etching step to remove the oxide layer.[4–11] In Si and Ge systems, atomic layer etching has been demonstrated using alternating stages of chlorine or fluorine adsorption, followed by a desorption of these reaction products by Ar^+ ion irradiation[12–16] or thermal methods.[17,18] However, no equivalent etch process has yet been demonstrated in the $Ge_{1-x}Sn_x$ system. In this work, we show that a two-step digital etch process consisting of a highly selective fluorine-based plasma etch followed by an acid wet etch can achieve consistent etch rates as low as 1.5 nm/cycle in $Ge_{0.922}Sn_{0.078}$.

$Ge_{0.922}Sn_{0.078}$ samples are grown using an Applied Materials Centura Epi Reduced-Pressure Chemical Vapor Deposition (RPCVD) system. A strain-relaxed 4 μm Ge buffer is grown on (001)-oriented Si using a multiple-step Ge growth and hydrogen anneal to provide a high-quality template with reduced lattice mismatch for $Ge_{1-x}Sn_x$ epitaxy.[19] A fully strained 30 nm layer of $Ge_{0.922}Sn_{0.078}$ is grown epitaxially using digermane (Ge_2H_6) and tin tetrachloride ($SnCl_4$) precursors at growth temperatures below 350 °C, followed by a 50 nm Ge cap. Figure 1(a) shows a high-resolution (004) ω-2θ scan by X-ray Diffraction (XRD). The presence of interference fringes surrounding the $Ge_{0.922}Sn_{0.078}$ peak suggests good interface quality. Due to thermal mismatch between Ge and Si during buffer growth, the Ge buffer retains a slight tensile strain of 0.166%. Furthermore, a two-dimensional reciprocal space map (RSM) in the (224) orientation shows alignment of both Ge and $Ge_{0.922}Sn_{0.078}$ peaks along the Q_x direction, confirming that the $Ge_{0.922}Sn_{0.078}$ is pseudomorphic to the underlying Ge buffer with excellent crystal quality (Figure 1(b)). The asymmetric (224) reflection shows that the $Ge_{0.922}Sn_{0.078}$ is under 0.97% compressive strain. Etch rate calibration in this work is carried out for fully strained $Ge_{0.922}Sn_{0.078}$ (referred to as GeSn for the remainder of the discussion) but is expected to vary with composition since the GeSn dry etch selectivity significantly depends on the Sn content within the material.[20]

a)Author to whom correspondence should be addressed. Electronic mail: ckshang@stanford.edu

 © 2016 AIP Publishing LLC

Reuse of AIP Publishing content is subject to the terms at: https://publishing.aip.org/authors/rights-and-permissions. Download to IP: 128.103.220.217 On: Thu, 26 May 2016 21:13:39

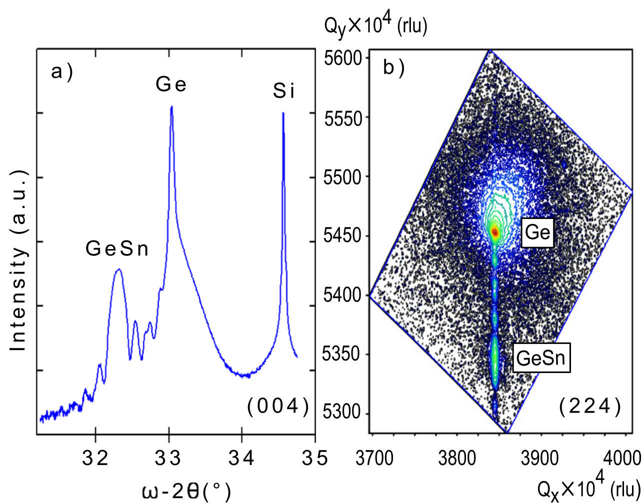

FIG. 1. High-resolution X-ray Diffraction for the as-grown material stack. (a) The ω-2θ line scan in the (004) orientation shows fringes surrounding the GeSn peak that indicate good interface quality. (b) Reciprocal space map of the (224) reflection shows the alignment of Ge and GeSn peak positions along Q_x and confirms that GeSn is pseudomorphic to Ge buffer with excellent crystal quality.

The digital etching process relies on two alternating and highly selective etch steps that enable precise and consistent material removal over each etch cycle. Prior to etching, the native oxide layers of all samples were removed using an acid dip in dilute hydrochloric acid (HCl). In the first step of the cycle, samples are placed in a Drytek plasma etcher (30 W) with 100 sccm of CF_4 (Freon-14/tetrafluoromethane). In this step, dissociated F radicals react with the GeSn surface forming both germanium tetrafluoride (GeF_4) and tin fluoride (SnF_y). The more volatile GeF_4 desorbs from the surface, while SnF_y remains as a passivating layer that strongly inhibits further etching of GeSn.[21] To reduce the effect of plasma damage to GeSn, a high pressure (700 mTorr) is selected. In the following step, HCl specifically removes the Sn-rich protective layer without further etching the underlying bulk GeSn. Samples are subject to a dilute acid treatment in a 1:1 v/v ratio of deionized (DI) water to 37% HCl for 15 s, rinsed in DI water, and fully dried with nitrogen before the next cycle. Each stage in the digital etch process is constrained to the GeSn surface and removes only the surface material each time. In this work, one etch cycle is defined as one CF_4 plasma etch followed by one HCl wet etch. Within the first cycle, the initial dry etching step is also used to etch away the Ge cap layer and expose the underlying GeSn to further etching cycles.

A Philips X'Pert Diffractometer was used to take X-ray Reflectivity (XRR) spectra, which were simulated and fit using a combination of genetic algorithm and segmented fit refinement in PANalytical X'Pert Reflectivity software. The technique measures the specular reflection of multilayer structures from low incidence angles to obtain information on film thickness, density, and surface or interface roughness independent of layer crystallinity. Unlike ellipsometry methods, distinct index contrast is not required in this approach which is better suited for the Ge/GeSn system. Moreover, the technique is non-destructive and does not require additional lithographic patterning for etch depth calibration, in contrast to atomic force microscopy or step profilometry methods.

In Figure 2, a series of XRR spectra are shown for four etch cycles using a dry etch duration of 60 s. Changes to the periodicity of reflection fringes are observed following each successive etch cycle which corresponds to a change in the remaining GeSn thickness. The amplitude variation of these fringes is attributed to the degree of contrast between layers, which can originate from density differences, interface roughness, or surface roughness. The enhancement after two etch cycles results from the change in surface topography, which is characterized by a negative surface roughness skew consisting of scattered pits or valleys in contrast to a positive skew for zero and one etch cycle. In particular, the plateau-like regions surrounding these pits exhibit a lower roughness than the positive roughness features found in zero and one etch cycle. Thus, a more rapid decay of reflected X-ray intensity occurs for the latter case and is likewise observed beyond three cycles. Despite apparent increases to surface roughness upon multiple etch cycles, the spacing of negative roughness features is comparable to the lateral coherence length of the X-ray beam, making it still possible to obtain specular reflection and layer thickness using XRR.

The extracted layer thicknesses from the XRR spectra are shown in Figure 3 along with the series for a 10 s dry etch time per cycle. For samples etched for 60 s, reliable reflectivity measurements could not be taken beyond four cycles due to high surface roughness. In both cases, a good linear fit is observed which confirms that a consistent depth of GeSn is etched away each cycle. The cycle etch rate extracted from the slope is 1.5 nm per cycle and 3.2 nm per cycle for 10 s and 60 s, respectively.

An ideal digital etch eliminates the requirement for timed etching if all processes are completely self-limiting. In the current case, the variation in etch rate observed between different dry etch durations is likely due to an additional physical sputtering component that can arise from the bombardment of a surface by energetic ions of the RF plasma. Although the formation of SnF_y inhibits further reactions between GeSn and F radicals, physical sputtering of this

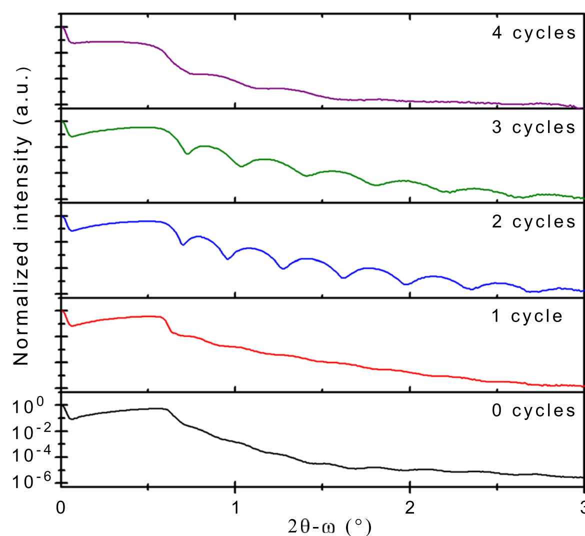

FIG. 2. X-ray Reflectivity 2θ-ω spectra shown for one through four etch cycles using a 60 s dry etch time. The normalized spectra have the same vertical axis scale and are offset for clarity. Changes to fringe periodicity with different etch cycles indicate different remaining GeSn thicknesses.

Reuse of AIP Publishing content is subject to the terms at: https://publishing.aip.org/authors/rights-and-permissions. Download to IP: 128.103.220.217 On: Thu, 26 May 2016 21:13:39

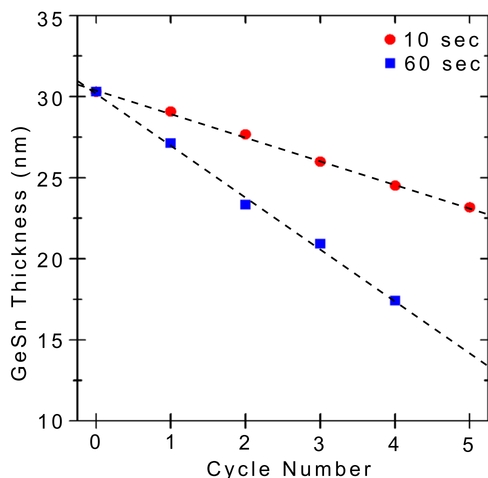

FIG. 3. Remaining GeSn layer thickness is determined by fitting XRR spectra and shown for one through five etch cycles using 10 s and 60 s dry etch times. Linear fitting of GeSn thickness versus cycle number (dashed lines) is used to extract cycle etch rates.

surface layer can still occur allowing continued GeSn etching below. For the 10 s CF_4 plasma etch, the depth of 1.5 nm removed each cycle is consistent with the estimated thickness of the passivating SnF_y surface layer (SnO_xF_y upon oxidation between dry and wet etch steps) estimated by Gupta *et al.* using X-ray Photoemission Spectroscopy.[21] This suggests that the dry etching step is still operating in the chemically self-limiting regime and forming an uncompromised SnF_y layer. However, for the longer dry etch time, physical sputtering of SnF_y and GeSn is no longer negligible and increases the etch rate to 3.2 nm per cycle. If this sputtering contribution is reduced such that GeSn etching occurs only via GeF_4 desorption until the formation of an undisrupted SnF_y layer, the cycle etch rate is not expected to vary with time.

Evidence of the enhanced sputtering over prolonged dry etch time is supported by the substantial increase in root-mean-square (RMS) surface roughness characterized by Non-Contact Atomic Force Microscopy (NC-AFM) and roughness extracted from simulated XRR spectra. In Figure 4(a), the 10 s etch series is characterized by little change in RMS roughness upon successive etch cycles which is consistent with an etch regime governed by the thickness of the protective SnF_y layer. However, the RMS roughness for the

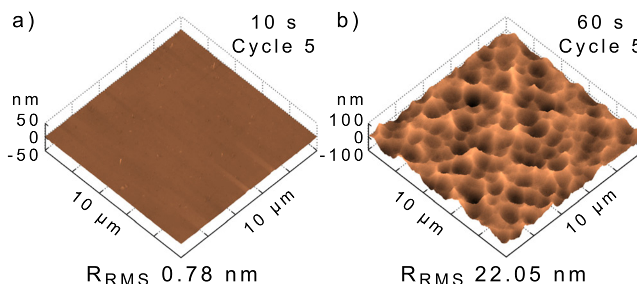

FIG. 5. Surface topography of GeSn characterized by NC-AFM after five etch cycles (a) Planar appearance with low RMS roughness of 0.78 nm using 10 s dry etch time (b) Dimpled appearance with high RMS roughness of 22.05 nm using 60 s dry etch time.

60 s etch series continues to increase following each cycle, which is uncharacteristic of a truly digital process. Even for comparable depths of material etched, the roughness is substantially larger as shown in the inset of Figure 4(a).

A comparison of one-dimensional line profiles from NC-AFM is also shown in Figure 4(b). Again, the surface profile for the 10 s series remains consistent between cycles while the 60 s series shows an increase in density and depth of pits. At the same time, surrounding regions still contribute reflected X-ray intensity though the inclusion of these pitted features in the calculation of RMS roughness increases the overall reported roughness of the surface. In addition, the absence of material as a result of these pits lowers the effective density of the GeSn film seen from XRR (right axis Figure 4(a)). Beyond three cycles, the roughness in some regions exceeds the film thickness and is no longer confined to GeSn, but also reaches the exposed Ge buffer layer. By five cycles, the RMS roughness reaches 22.05 nm and the surface exhibits a more dimpled appearance in contrast to the planar appearance observed for the shorter etch time reaching an RMS roughness of 0.78 nm (Figure 5).

Thus an increase in etch rate comes at the cost of enhanced roughness and surface damage. For a given depth of GeSn to be removed, operating in a dry etching regime governed by GeF_4 desorption instead of sputtering offers the most precise etch control with minimal change in surface quality, but at the requirement of increased etching cycles. Lowering RF power in the dry etch process can reduce surface damage but leads to a decreased etch rate.[21]

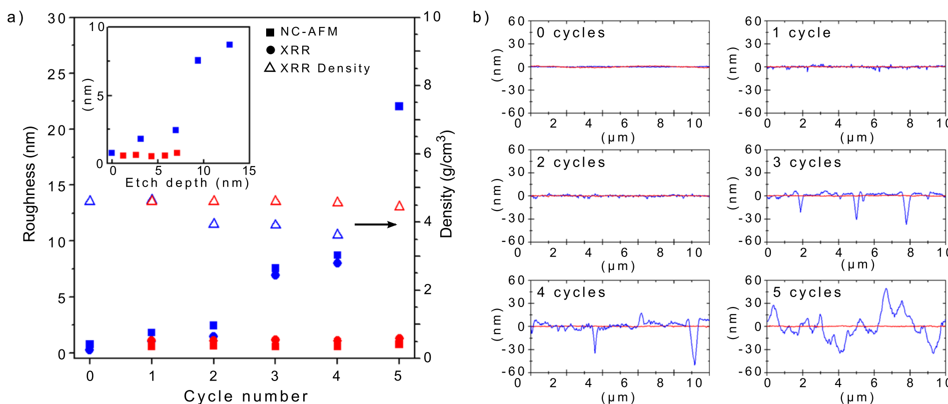

FIG. 4. (a) Left axis: Surface roughness from NC-AFM and XRR for dry etch times of 10 s (red) and 60 s (blue). Roughness is reduced with the shorter dry etch time since etching relies on GeF_4 desorption rather than additional physical sputtering. Right axis: GeSn film density obtained from simulated XRR spectra decreases with negative roughness skew. Inset: RMS roughness (nm) plotted versus etch depth over cumulative cycles confirms that for a given depth, GeF_4 desorption rather than physical sputtering maintains better surface quality. (b) NC-AFM surface profiles for both etch times and all cycles.

Reuse of AIP Publishing content is subject to the terms at: https://publishing.aip.org/authors/rights-and-permissions. Download to IP: 128.103.220.217 On: Thu, 26 May 2016 21:13:39

In summary, we demonstrate digital etching of GeSn (7.8% Sn) based on highly selective alternating CF_4 plasma dry etching and HCl wet etching. Consistent etch rates were found for both 10 s and 60 s of dry etching times at 1.5 nm and 3.2 nm per cycle, respectively. For longer dry etch duration, increased surface roughness and cycle etch rate were attributed to a physical sputtering component in addition to the chemical etching process. To achieve a given etch depth, a greater number of etch cycles with reduced plasma etching time yields optimal etch control and surface quality. This technique extends the utility of the known etch stop behavior exhibited in this system and has the potential to enable the design, fabrication, and optimization of $Ge_{1-x}Sn_x$-based devices.

The authors acknowledge financial support from the Advanced Photonic Integrated Circuits (APIC) Corporation, the Vice Provost for Undergraduate Education, and Undergraduate Advising and Research at Stanford University. The authors also thank Dr. Arturas Vailionis for discussions on XRR. Work was performed at the Stanford Nano Shared Facilities and the Stanford Nanofabrication Facility supported by the National Science Foundation, through the National Nanotechnology Infrastructure Network under Grant No. ECS-9731293.

[1]S. Gupta, B. Magyari-Köpe, Y. Nishi, and K. C. Saraswat, J. Appl. Phys. **113**, 073707 (2013).
[2]R. Chen, H. Lin, Y. Huo, C. Hitzman, T. I. Kamins, and J. S. Harris, Appl. Phys. Lett. **99**, 181125 (2011).
[3]S. Wirths, R. Geiger, N. von den Driesch, G. Mussler, T. Stoica, S. Mantl, Z. Ikonic, M. Luysberg, S. Chiussi, J. M. Hartmann, H. Sigg, J. Faist, D. Buca, and D. Grützmacher, Nat. Photonics **9**, 88 (2015).
[4]K. Hennessy, A. Badolato, A. Tamboli, P. M. Petroff, E. Hu, M. Atatüre, J. Dreiser, and A. Imamoğlu, Appl. Phys. Lett. **87**, 021108 (2005).
[5]T. Sünner, R. Herrmann, A. Löffler, M. Kamp, and A. Forchel, Microelectron. Eng. **84**, 1405 (2007).
[6]D. Buttari, S. Heikman, S. Keller, and U. K. Mishra, in *IEEE Lester Eastman Conference on High Performance Devices* (2002), pp. 461–469.
[7]X. Cao and I. Thayne, Microelectron. Eng. **67–68**, 333 (2003).
[8]S. Lee, C.-Y. Huang, A. D. Carter, J. J. M. Law, D. C. Elias, B. J. Thibeault, W. Mitchell, S. Stemmer, A. C. Gossard, and M. J. W. Rodwell, in *Conference Proceedings of Indium Phosphate* (2013), Vol. 1, pp. 7–8.
[9]G. C. DeSalvo, C. A. Bozada, J. L. Ebel, D. C. Look, J. P. Barrette, C. L. Cerny, R. W. Dettmer, J. K. Gillespie, C. K. Havasy, T. J. Jenkins, K. Nakano, C. I. Pettiford, T. K. Quach, J. S. Sewell, and G. D. Via, J. Electrochem. Soc. **143**, 3652 (1996).
[10]T. Meguro, M. Hamagaki, S. Modaressi, T. Hara, Y. Aoyagi, M. Ishii, and Y. Yamamoto, Appl. Phys. Lett. **56**, 1552 (1990).
[11]J. Lin, X. Zhao, D. A. Antoniadis, and J. A. del Alamo, IEEE Electron Device Lett. **35**, 440 (2014).
[12]H. Sakaue, S. Iseda, K. Asami, J. Yamamoto, M. Hirose, and Y. Horiike, Jpn. J. Appl. Phys., Part 1 **29**, 2648 (1990).
[13]J. Yamamoto, T. Kawasaki, H. Sakaue, S. Shingubara, and Y. Horiike, Thin Solid Films **225**, 124 (1993).
[14]T. Matsuura, J. Murota, Y. Sawada, and T. Ohmi, Appl. Phys. Lett. **63**, 2803 (1993).
[15]K. Suzue, T. Matsuura, J. Murota, Y. Sawada, and T. Ohmi, Appl. Surf. Sci. **82–83**, 422 (1994).
[16]K. J. Kanarik, S. Tan, J. Holland, A. Eppler, V. Vahedi, J. Marks, and R. A. Gottscho, Solid State Technol. **56**, 14 (2013).
[17]S. Imai, T. Haga, O. Matsuzaki, T. Hattori, and M. Matsumura, Jpn. J. Appl. Phys., Part 1 **34**, 5049 (1995).
[18]K. Ikeda, S. Imai, and M. Matsumura, Appl. Surf. Sci. **112**, 87 (1997).
[19]D. Choi, Y. Ge, J. S. Harris, J. Cagnon, and S. Stemmer, J. Cryst. Growth **310**, 4273 (2008).
[20]Y. Dong, D. Lei, X. Xu, W. Wang, and Y.-C. Yeo, in *International Silicon-Germanium Technology and Device Meeting* (2014), pp. 99–100.
[21]S. Gupta, R. Chen, Y.-C. Huang, Y. Kim, E. Sanchez, J. S. Harris, and K. C. Saraswat, Nano Lett. **13**, 3783 (2013).

Reuse of AIP Publishing content is subject to the terms at: https://publishing.aip.org/authors/rights-and-permissions. Download to IP: 128.103.220.217 On: Thu, 26 May 2016 21:13:39